ISSN 1063-7834, Physics of the Solid State, 2021, Vol. 63, No. 2, pp. 242–247. © Pleiades Publishing, Ltd., 2021.
Russian Text © The Author(s), 2021, published in Fizika Tverdogo Tela, 2021, Vol. 63, No. 2, pp. 218–223.

SEMICONDUCTORS

Magnetoresistance and IR Spectrum of Impurity States in the $Ce_3Fe_5O_{12}$ Film

S. S. Aplesnin[a, b, *], A. N. Masyugin[a], V. V. Kretinin[a], S. O. Konovalov[a], and N. P. Shestakov[b]

[a] *Reshetnev Siberian State University of Science and Technology, Krasnoyarsk, 660037 Russia*

[b] *Kirensky Institute of Physics, Krasnoyarsk Scientific Center, Siberian Branch, Russian Academy of Sciences, Krasnoyarsk, 660036 Russia*

**e-mail: apl@iph.krasn.ru*

Received October 18, 2020; revised October 18, 2020; accepted October 20, 2020

Abstract—In polycrystalline cerium iron garnet films, the gap in the electron excitation spectrum and electronic transitions between di- and tetravalent iron and cerium impurity ions have been established from the IR absorption spectra. The temperatures of delocalization of the ferrous states of iron have been found from the impedance spectroscopy, electrical resistance, and IR spectroscopy data. The difference between the ac and dc magnetoresistances has been established and explained using a model of a dielectrically inhomogeneous medium.

Keywords: magnetoimpedance, IR spectroscopy, cerium iron garnet, thin films

DOI: 10.1134/S1063783421020025

1. INTRODUCTION

The iron garnet films with rare-earth cations are promising for application in magnetooptics [1–3], including magneto-plasmonic photonics [4] and fabrication of magnonic crystals [5]. Polycrystalline films are inferior in characteristics to their bulk analogs, but exhibit the resistance to the formation of microelectronic structures based on them. Nanostructured yttrium iron garnet (YIG) [6, 7] has been intensively investigated, which is important for both solving the fundamental problems of physics of nanocrystalline magnets and application in coatings and nanocomposites containing piezoelectric materials with the colossal magnetoelectric effect [8–10]. Nanomaterials are nonequilibrium systems with the high imperfection. Point and other defects strongly affect the optical and magnetic properties of YIG [11].

YIG nanoceramics prepared by high-pressure torsion exhibit the strong imperfection caused by the violation of stoichiometry and valence state of iron cations [11]. The divalent state of iron ions is formed upon doping of YIG with tetravalent ions, which occupy the octahedral sites. The presence of Fe^{2+} ions leads to the negative magnetic dichroism in Nb(YIG) [12]. These ions form the impurity states in the band gap and two conduction channels in the iron garnet structure. One conduction channel is related to electron transport over the *t2g* states of Fe^{2+} ions and a rare-earth element Re in the octahedral sites; the other channel is related to electron transport over tetrahedra with the creation of magnons on a rare-earth element. The transitions of electrons between iron ions in the tetra- and octahedral sites are associated with the creation of magnons and possibility of formation of a magnon cloud (ferrons) [13, 14] upon approaching the temperature of the magnetic phase transition. In this case, the transport properties will depend on a magnetic field. The formation of Fe^{2+} in iron garnets can also be caused by charge fluctuations. In particular, cerium iron garnets exhibit the charge fluctuations $Ce^{+3} - Fe^{+3} = Ce^{+4} - Fe^{+2}$ with a gap of 1.3 eV [15]. At the interface and grain boundaries, fluctuations of the crystal field will lead to a decrease in the gap. Cerium ions in $CeFe_2$ have an intermediate valence of 3.4 [16]. The valence fluctuations upon substitution of cerium for yttrium can enhance the conductivity over its value for $Y_3Fe_5O_{12}$.

The aim of this study was to elucidate the defect states of ions and the magnetoresistive effects in the polycrystalline $Ce_3Fe_5O_{12}$ film.

2. X-RAY DIFFRACTION ANALYSIS AND IR AND OPTICAL SPECTROSCOPY

Layers with the nominal composition $Ce_3Fe_5O_{12}$ were obtained by ion-beam sputtering onto a gallium gadolinium garnet (GGG) substrate [17]. A 400-nm-thick film was polycrystalline with an average grain size of 60–70 nm.

The X-ray diffraction pattern of the $Ce_3Fe_5O_{12}$ film is shown in Fig. 1. The film has a cubic structure

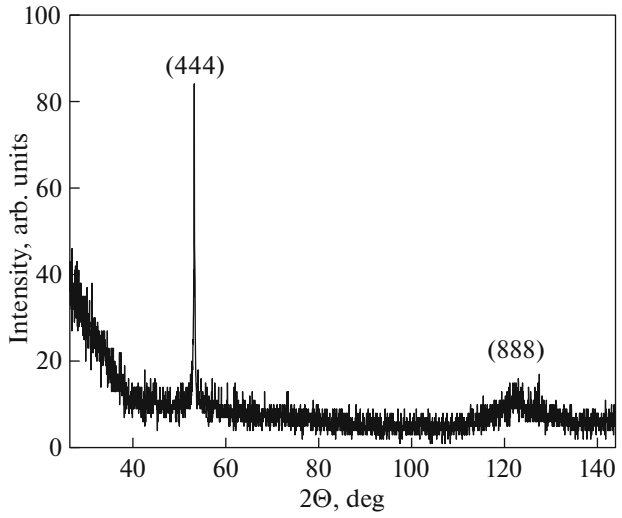

Fig. 1. X-ray diffraction pattern of the $Ce_3Fe_5O_{12}$ film.

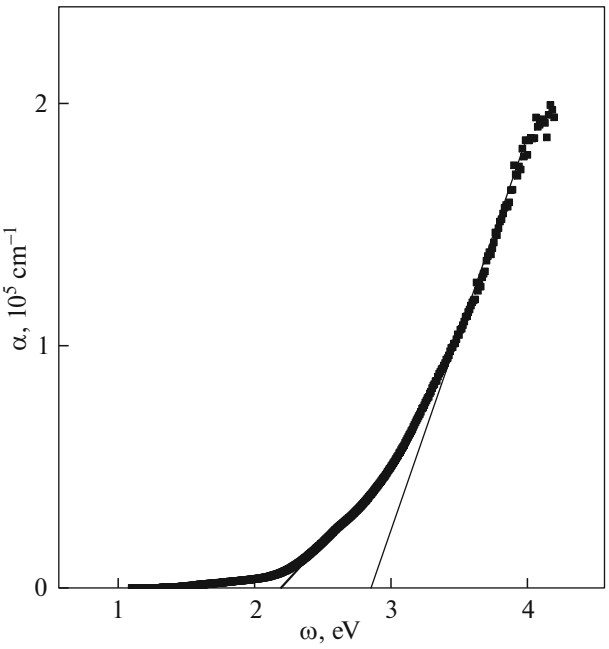

Fig. 2. Absorption spectrum of the $Ce_3Fe_5O_{12}$ film as a function of the photon energy.

(sp. gr. *Ia*3*d*(230)) with a preferred orientation in the (444) direction. The parameter of the cubic unit cell of the film is $a = 1.234$ nm. The crystal structure of the film is noticeably strained ($\Delta a = a_{substrate} - a_{film} = 0.05$ Å). The difference between the film and substrate lattice parameters is ~0.4%.

The optical absorption spectrum was recorded on a Cary500Scan spectrophotometer (Fig. 2). The band gap is $E_g = 2.78$ eV [18].

Substitution of cerium for yttrium leads to a slight decrease in the band gap as compared with a value of $E_g = 2.85$ eV for $Bi_3Fe_5O_{12}$ [19] and 3.1 eV for YIG on garnet. The tails in the range of 2–2.8 eV are caused by the transition of electrons in the crystal field of the tetrahedron with Fe^{3+} between the multiplets ${}^6A_1 \rightarrow {}^4T_2$, ${}^4A_1$, ${}^4E$, ${}^4T_2$, ${}^4T_1$, and ${}^4E$. An electronic transition with the charge transfer $2p$–$3d$ between iron ions in the octahedral and tetrahedral sites occurs at 2.8 eV.

We determine the charged defect states from the IR spectra (Fig. 3a). The IR spectrum contains two absorption lines in the frequency range of $\omega_1 \sim 5520$ cm^{-1} ($\lambda_1 \sim 1.5$ μm) and $\omega_2 \sim 6800$ cm^{-1} ($\lambda_1 \sim 1.8$ μm). One line at frequency ω_1 disappears at 275 K and the other line at frequency ω_2, in the temperature range of 360–400 K. Two transition lines at wavelengths of 1.95 and 2.15 μm were observed for $Y_3Fe_5O_{12}$ (YIG) doped with tetravalent Zr [20] and Pb ions [21]. The explanation made in [22] concerned the optical transitions in a divalent iron ion in a low-symmetry crystal field. The triplet ${}^5T_{2g}$ state of Fe^{2+} ions in an octahedron (tetrahedron) with the triclinic lattice distortion is split into the doublet ${}^5E_{g1}$ and the singlet A_g. In the model of the crystal field with the parameters $10D_q = 9500$ cm^{-1} and a trigonal splitting of $C = 500$ cm^{-1}, the electronic transition to $A_g - 5E_g$ at a wavelength of 1.54 μm in the octahedron and at 1.66 μm in the tetrahedron was calculated. The wavelengths depend on the crystal field parameters and the positions of Fe^{2+} ions, on defects. With the change in the symmetry from trigonal to cubic, these transitions vanish. In $(Y_{1-x}Ce_x)Fe_5O_{12}$, the crystal symmetry does not change above 170 K [23]. It can be assumed that crystalline phase transitions do not occur in the $Ce_3Fe_5O_{12}$ films upon heating.

The electronic transitions can be induced by the charge fluctuations of cerium ions $Ce^{3+} + Fe^{3+} \rightarrow Ce^{4+} + Fe^{2+}$ with an ion recharging energy of 1.2 eV in the bulk of the crystal. On the film surface or near defects with the violation of the coordination number of the nearest neighbors, Ce^{4+} and Fe^{2+} ions can exist, which were found in tetrahedra by the Mössbauer technique [24]. According to ab initio calculations, the energy of the charge redistribution on the Ce–O bond ranges between 0.54–0.7 eV [25]. The ionic radius of cerium Ce^{3+} (1.14 Å) is greater than the Ce^{4+} radius (0.97 Å) and the Fe^{2+} radius (0.63 Å) is greater than the Fe^{3+} radius (0.49 Å) in the tetrahedral site. The charge transfer leads to the shortening of the Ce–O bond length. The *d*–*f* dipole electronic transitions between Fe^{2+} ions in the tetrahedral (octahedral) sites and Ce^{4+} form two absorption lines.

The absorption line at frequency ω_1 disappears at 275 K due to electron delocalization near the Ce^{4+}, Fe^{2+} pair in the octahedron upon straining the film relative to the substrate. Delocalization of electrons on

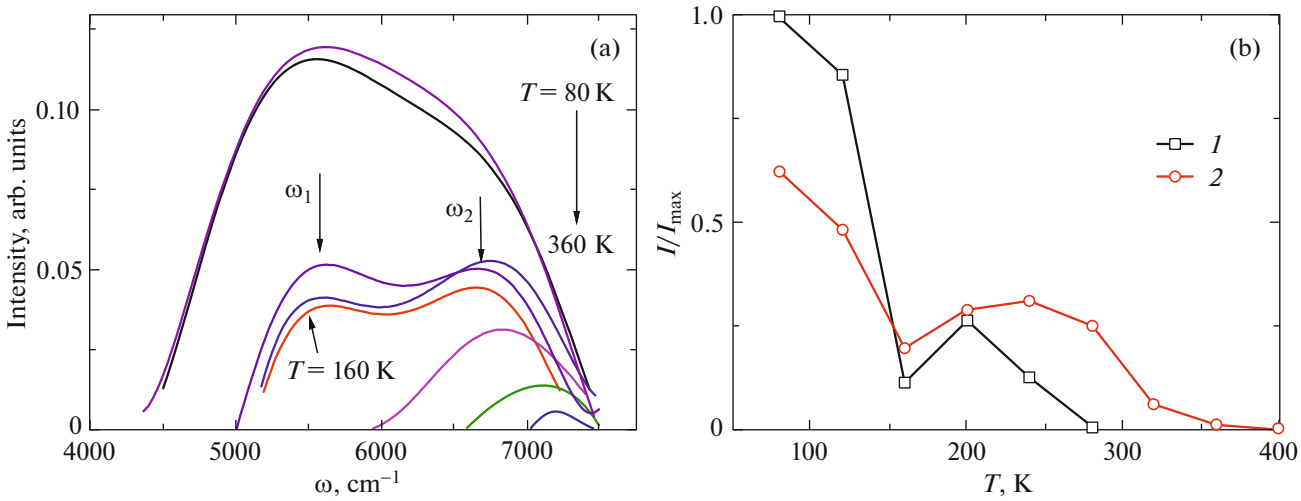

Fig. 3. (a) IR absorption of the $Ce_3Fe_5O_{12}$ film in the frequency range of 4500–7500 cm^{-1}. (b) Absorption intensity at frequencies (*1*) ω_1 and (*2*) ω_2 vs temperature.

Fe^{2+} in the tetrahedron above 360 K leads to the disappearance of the transition at frequency ω_2. Further heating leads to the electron hopping between Fe^{2+} ions in the tetrahedral sites and Fe^{3+} ions in the octahedral sites. The temperature 160 K at which the intensity of IR absorption of the $Ce_3Fe_5O_{12}$ film sharply drops (Fig. 3b) is consistent with the temperature 170 K of the spin-reorientation transition in $(Y_{1-x}Ce_x)Fe_5O_{12}$ [23].

3. ELECTRICAL RESISTANCE, I–V CHARACTERISTICS, AND IMPEDANCE

The electrical resistance was measured by a four-point probe method. The film is high-ohmic and the resistance detection starts with 2 GΩ above 350 K (Fig. 4).

At 400 K, the activation energy decreases from 0.27 to 0.18 eV. The ac resistance increases upon heating and reaches a local maximum with a plateau also at 400 K, where the impedance has a minimum (Fig. 5). The impedance minimum is related to the disappearance of migration polarization due to electron delocalization.

Figure 6 shows frequency dependences of the impedance components in the frequency range of 10^2–10^6 Hz. The impedance is well-described by the power function of the frequency $Z = A/\omega^n$. The reactive resistance is determined by the inductive contribution $X_L = L\omega$ and the capacitive contribution $X_c = 1/C\omega$. Fitting of the experimental data yields $n = 1.0 \pm 0.02$ in the temperature range of 300–500 K. In other words, the reactance is determined by the localized charges and the film capacitance C: $\mathrm{Im}Z(\omega) = 1/C\omega$. The impedance minimum at 400 K is related to the maximum capacitance caused by the disappearance of dipole moments of the Ce^{4+}, Fe^{2+} pairs in the tetrahedron. The impedance variation in a magnetic field is no more than 0.1%. The active resistance is also described by the power dependence $\mathrm{Re}(Z(\omega)) = B/\omega^n$, where the exponent increases from $n = 0.95 \pm 0.04$ to 1.22 ± 0.03 upon heating to 500 K. The resistance depends on the measuring frequency, which is indicative of the hopping mechanism of charge transfer. In this case, the frequency dependence of the conductivity is described by the expression $\sigma = \sigma_0\omega^s$, where $s = 0.8$ [26], which corresponds to the hopping recharging of one-type defects. The ac resistance increases in a magnetic field and decreases above 450 K (Fig. 7).

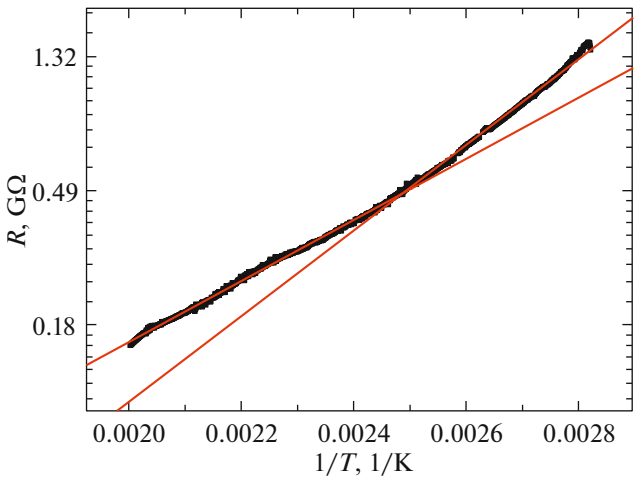

Fig. 4. Resistance of the $Ce_3Fe_5O_{12}$ film vs reciprocal temperature.

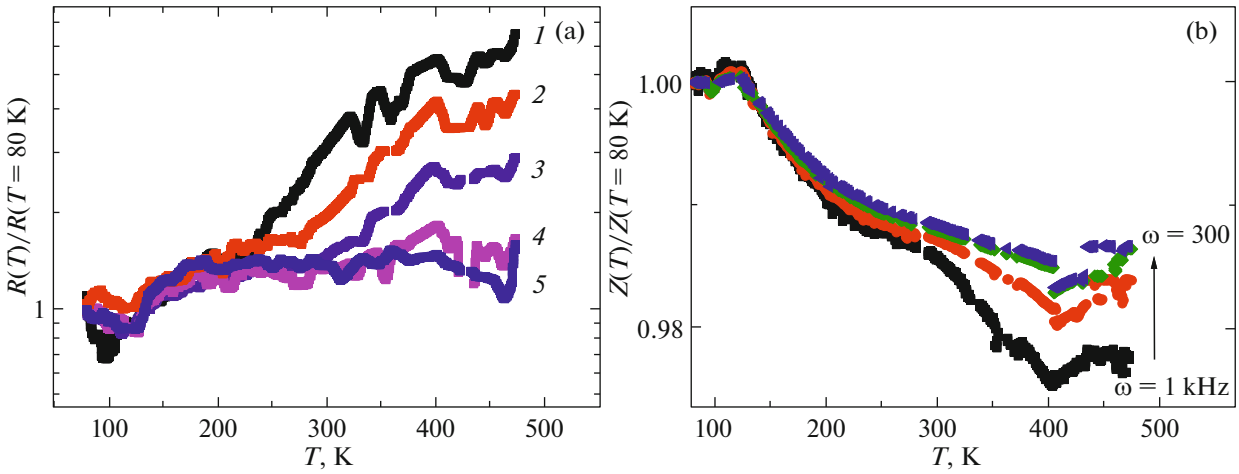

Fig. 5. (a) Normalized real part of the impedance Re($Z(T = 80$ K) and (b) impedance $Z(T = 80$ K) vs temperature at frequencies of ω = (*1*) 1, (*2*) 5, (*3*) 10, (*4*) 50, (*5*) 100, and (*6*) 300 kHz.

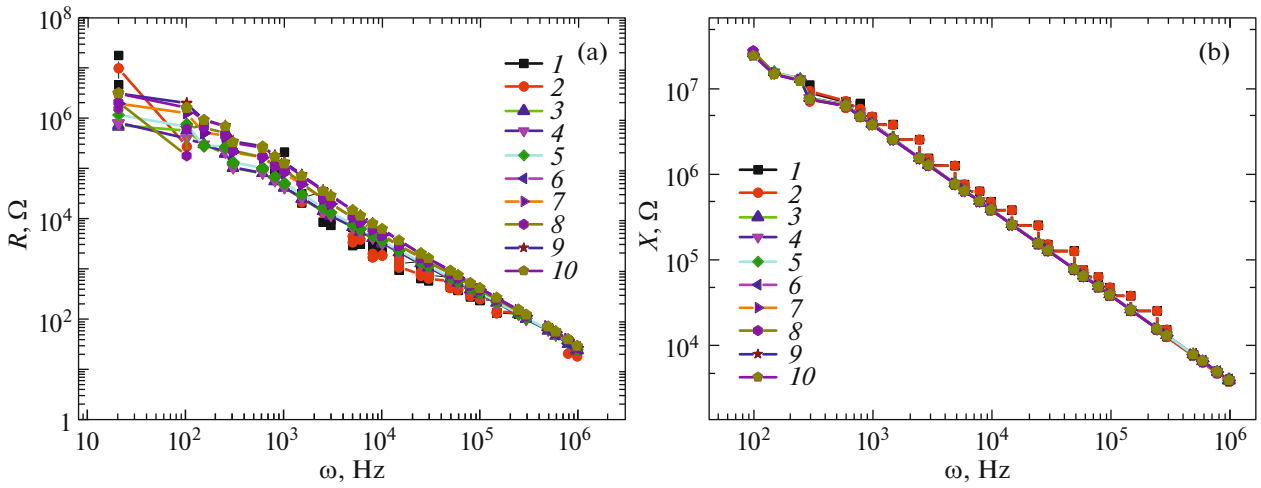

Fig. 6. (a) Active and (b) reactive resistance of the $Ce_3Fe_5O_{12}$ film (*1*, *3*, *5*, *7*, *9*) without field and (*2*, *4*, *6*, *8*, *10*) in a magnetic field of 8 kOe at temperatures of $T = $ (*1*, *2*) 300, (*3*, *4*) 350, (*5*, *6*) 400, (*7*, *8*) 450, and (*9*, *10*) 500 K.

The I–V characteristics of the films in the temperature range of 300–500 K and magnetic fields of up to 8 kOe are presented in Fig. 8. The $I(U)$ dependences are linear and antihysteretic. The conductivity obeys the Ohm's law. The change in the current (resistance) in a magnetic field is no more than 0.5%. The dc magnetoresistance is lower than the ac magnetoresistance by an order of magnitude.

4. MODEL

The temperature dependences of the IR spectra and conductivity can be explained by the presence of divalent iron ions. Upon doping with cerium (Ce:YIG/GGG), the films exhibit the rhombohedral distortion and the change in the mutual arrangement of octahedra and tetrahedra [23, 27]. Tetrahedra are more prone to straining than octahedra. The pseudocubic lattice constant increases upon heating above 170 K; at this temperature, the spin-reorientation transition from the easy axis to the easy plane occurs [23]. The IR spectra include two absorption lines corresponding to the transition of electrons between Fe^{2+} cations in octahedra and tetrahedra and the Ce^{4+} ion. A change in the angle of the rhombohedral distortion leads to a change in the angle between the Fe^{2+}–O and O–Ce^{4+} bonds and the height of the potential barrier for electron tunneling between cations. A sharp decrease in the intensity of electronic transitions in the IR spectra is caused by a decrease in

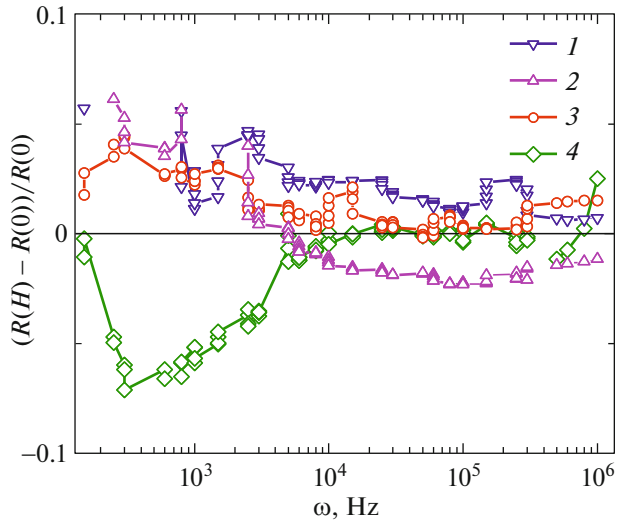

Fig. 7. Frequency dependence of magnetoresistance $((R(H) - R(0))/R(0)$ at $T = (1)$ 300, (2) 350, (3) 450, and (4) 500 K.

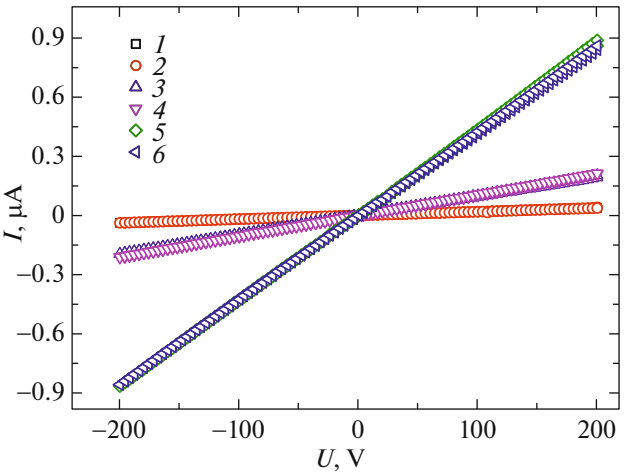

Fig. 8. I–V characteristics of the $Ce_3Fe_5O_{12}$ film $(2, 4, 6)$ without field and $(1, 3, 5)$ in a magnetic field of 8 kOe at temperatures of $T = (1, 2)$ 400, $(3, 4)$ 450, and $(5, 6)$ 500 K.

the tunneling coefficients $D_1/D_2 = \exp(\Delta_2 - \Delta_1) \sim 5$ in the vicinity of 160 K.

Upon heating above 160 K, a tangential voltage component along the film–substrate interface appears. For example, in Ce:YIG/GGG, the thermal expansion coefficient of the film grows faster than that of the substrate at $T > 170$ K, passes through a maximum at 210 K, and changes its sign at 284 K. The change in the sign of the elastic stress from the substrate side to the film leads to delocalization of an electron in Fe^{2+} in the octahedron. One absorption line remains in the IR spectrum at the transition of electrons between Fe^{2+} and Ce^{4+} cations in the tetrahedron. In the temperature range of 360–400 K, the charge fluctuations $Ce^{4+} + Fe^{2+} \rightarrow Ce^{3+} + Fe^{3+}$ are enhanced, which leads to the disappearance of the absorption line at frequency ω_2.

Let us consider the qualitative difference between the dc and ac magnetoresistances, which differ by more than an order of magnitude. The ac conductivity in a disordered medium is related to the dielectric constant $\sigma(\omega, \mathbf{r}) = i\omega\varepsilon(\omega, \mathbf{r})$, where σ is the conductivity tensor and ε is the local dielectric function. In the approximation of $1/\omega$ longer than the scattering time, the conductivity tensor in the transverse magnetic field H^Z is

$$\hat{\sigma}(\omega) = \frac{\sigma}{1+\beta^2}\begin{pmatrix} 1 & \beta \\ -\beta & 1 \end{pmatrix} + i\omega\varepsilon, \qquad (1)$$

where $\beta = \mu H$ and μ is the mobility. At the hopping conductivity with the uniform distribution of carriers in the film, the diagonal component of the conductivity depends on frequency via the longitudinal dielectric response [28]

$$\mathrm{Re}[\varepsilon_{xx}(\omega)] = \frac{\varepsilon(1-\beta^2+(\omega\tau)^2(1+\beta^2)^2)}{1+(\omega\tau)^2(1+\beta^2)^2}, \qquad (2)$$

where $\tau = \varepsilon/\sigma$. As the field increases, the ε_{xx} decreases and the resistance in a magnetic field increases. Upon approaching the Curie temperature, the formation of ferrons is observed, which represent areas of local ferromagnetic ordering of spins in the tetrahedral and octahedral sites. The presence of electrically inhomogeneous states leads to an increase in the permittivity in a magnetic field. For a two-phase system with limiting parameters of $\sigma_1 = 0$, $\varepsilon = \varepsilon_1$ and concentration x and with $\sigma_2 = \sigma$, $\varepsilon = 0$ $(1 - x)$, we found a numerical solution for the dielectric response upon frequency variation in fixed magnetic fields in a 2D two-component medium, which can be approximated as $\varepsilon(\beta, \omega) \sim (\omega) + A(\omega)\beta^{1/2}$ [28].

5. CONCLUSIONS

Two absorption lines were found in the IR spectrum and temperatures of their disappearance were determined, which were attributed to the electronic transitions between impurity states of ferrous ions in the octahedral (tetrahedral) sites and tetravalent cerium. The temperature of the impedance minimum and the change in the activation energy caused by the disappearance of the migration polarization were established. A change in the ac magnetoresistance sign upon approaching the Curie temperature was observed and explained by the formation of electrically inhomogeneous states.

ACKNOWLEDGMENTS

We are grateful to A.I. Strognii, Scientific and Practical Materials Research Center, National Academy of Sciences of Belarus, for providing us with the samples.

FUNDING

This study was supported by the Russian Foundation for Basic Research, the Government of the Krasnoyarsk Krai, and the Krasnoyarsk Territorial Foundation for Support of Scientific and R&D Activities, project no. 18-42-240001 "Inversion of the Sign of Magnetoelectric Tensor Components with Temperature in the Neodymium-Doped Bismuth Iron Garnet Films."

CONFLICT OF INTEREST

The authors declare that they have no conflicts of interest.

REFERENCES

1. X. Ma, J. Mater. Sci.: Mater. Electron. **11**, 351 (2000).
2. M. C. Onbasli, T. Goto, X. Sun, N. Huynh, and C. A. Ross, Opt. Express **22**, 25183 (2014).
3. M. Huang and S.-Y. Zhang, Appl. Phys. A **74**, 177 (2002).
4. M. Vasiliev, P. C. Wo, K. Alameh, P. Munroe, Z. Xie, V. A. Kotov, and V. I. Burkov, J. Phys. D **42**, 135003 (2009).
5. A. B. Ustinov, A. V. Drozdovskii, A. A. Nikitin, A. A. Semenov, D. A. Bozhko, A. A. Serga, B. Hillebrands, E. Lähderanta, and B. A. Kalinikos, Commun. Phys. **2**, 1 (2019).
6. J. W. Lee, J. H. Oh, J. C. Lee, and S. C. Choi, J. Magn. Magn. Mater. **272–276**, 2230 (2004).
7. X. Z. Guo, B. G. Ravi, Q. Y. Yan, R. J. Gambino, S. Sampath, and J. Margolies, J. Parise Ceram. Int. **32**, 61 (2006).
8. A. M. J. G. Run, D. R. Terrell, and J. H. Scholing, J. Mater. Sci. **9**, 1710 (1974).
9. J. Boomgaard, A. M. J. G. Run, and J. Suhtelen, Ferroelectrics **10**, 295 (1976).
10. A. E. Gelyasin, V. M. Laletin, and L. I. Trofimovich, Sov. Tech. Phys. **33**, 1361 (1988).
11. B. A. Gizhevskii, Yu. P. Sukhorukov, E. A. Gan'shina, N. N. Loshkareva, A. V. Telegin, N. I. Lobachevskaya, V. S. Gaviko, and V. P. Pilyugin, Phys. Solid State **51**, 1836 (2009).
12. B. Antonini, S. Geller, A. Paoletti, P. Paroli, and A. Tucciarone, Phys. Rev. Lett. **41**, 1556 (1978).
13. E. L. Nagaev, Sov. Phys. Usp. **18**, 863 (1975).
14. M. Yu. Kagan and K. I. Kugel', Phys. Usp. **44**, 553 (2001).
15. M. Huang and S.-Y. Zhang, Appl. Phys. A **74**, 177 (2002).
16. Yu. P. Smirnov, A. E. Sovestnov, A. V. Tyunis, and V. A. Shaburov, Phys. Solid State **40**, 1269 (1998).
17. G. D. Nipan, A. I. Stognij, and V. A. Ketsko, ChemInform **44** (2) (2013).
18. J. I. Pankove, *Optical Processes in Semiconductors* (Prentice-Hall, Englewood Cliffs, 1971).
19. S. H. Wemple, S. L. Blank, J. A. Seman, and W. A. Biolsi, Phys. Rev. B **9**, 2134 (1974).
20. F. Lucari, C. Mastrogiuseppe, E. Terrenzio, and G. Tomassetti, J. Magn. Magn. Mater. **20**, 84 (1980).
21. F. Lucari, C. Mastrogiuseppe, and G. Tomassetti, J. Phys. C **10**, 4869 (1977).
22. Z. V. Gareyeva and R. A. Doroshenko, J. Magn. Magn. Mater. **268**, 1 (2004).
23. E. Lage, L. Beran, A. U. Quindeau, L. Ohnoutek, M. Kucera, R. Antos, S. R. Sani, G. F. Dionne, M. Veis, and C. A. Ross, APL Mater. **5**, 036104 (2017).
24. X. Guo, A. H. Tavakoli, S. Sutton, R. K. Kukkadapu, L. Qi, A. Lanzirotti, M. Newville, M. Asta, and M. Navrotsky, Chem. Mater. **26**, 1133 (2014).
25. M. M. Branda, C. Loschen, K. M. Neyman, and F. Illas, J. Phys. Chem. C **112**, 17643 (2008).
26. S. N. F. Mott, and E. A. Davis, *Electronic Processes in Noncrystalline Materials* (Clarendon, Oxford, 1971).
27. A. Kehlberger, K. Richter, M. C. Onbasli, G. Jakob, D. H. Kim, T. Goto, C. A. Ross, G. Götz, G. Reiss, T. Kuschel, and M. Kläui, Phys. Rev. Appl. **4**, 014008 (2015).
28. M. M. Parish and P. B. Littlewood, Phys. Rev. Lett. **101**, 166602 (2008).

Translated by E. Bondareva